# Phase Linearity Measurement: A Novel Index for Brain Functional Connectivity

Fabio Baselice, Antonietta Sorriso, Rosaria Rucco, and Pierpaolo Sorrentino

***Abstract*— The problem of describing how different brain areas interact between each other has been granted a great deal of attention in the last years. The idea that neuronal ensembles behave as oscillators and that they communicate through synchronization is now widely accepted. To this regard, EEG and MEG provide the signals that allow the estimation of such communication in vivo. Hence, phase-based metrics are essential. However, the application of phased-based metrics for measuring brain connectivity has proved problematic so far, since they appear to be less resilient to noise as compared to amplitude-based ones. In this paper, we address the problem of designing a purely phase-based brain connectivity metric, insensitive to volume conduction and resilient to noise. The proposed metric, named phase linearity measurement (PLM), is based on the analysis of similar behaviors in the phases of the recorded signals. The PLM is tested in two simulated datasets as well as in real MEG data acquired at the Naples MEG center. Due to its intrinsic characteristics, the PLM shows considerable noise rejection properties as compared to other widely adopted connectivity metrics. We conclude that the PLM might be valuable in order to allow better estimation of phase-based brain connectivity.**

***Index Terms*— Brain functional connectivity, functional coupling, phase metric, EEG, MEG, volume conduction.**

## I. Introduction

MANY of the complex functions of the brain cannot be explained by the activity of a single cell or neuronal ensemble. Instead, they become possible when many groups of neurons interact simultaneously [1]. The description of such interactions yields relevant information about the functioning of the brain in health and disease [2]. The term "connectivity" refers to the estimation of such interactions based upon statistical dependencies [3]. Recently, a number of connectivity metrics have been developed to capture various aspects of such statistical dependencies [4]. The choice of a specific metric depends upon the system being used to acquire the measurements of the brain (and hence the characteristics of the signal) and upon the hypothesis that is being tested [5]. Connectivity metrics can be classified into amplitude based measures, phase based measures or joint amplitude - phase measures [6]. Metrics based on amplitude quantify power correlations between time series [5]. Phase based measures consider signal phase changes related to information transfer between neurons or brain areas [7]. Indeed, one of the underlying assumptions usually applied when using phase based metrics is that synchronization is a way neuronal ensembles use to communicate [8]. There is a wide body of well-established literature that has proven to be able to predict synchronization phenomena under certain assumptions. One of this assumptions has been that the oscillators to be synchronized would display exactly the same dynamics. Such assumption has proven extremely useful and has simplified the math describing such systems [9]–[11], allowing models that precisely predict the states of a system of (weakly coupled) oscillators based on their phases. The observation that even single neurons display properties of oscillators, such as resonance and oscillations at multiple frequencies, has supported the use of such metrics to describe neural synchronization, and this has been done with great success [7]. However, the validity of the assumptions made to study simple systems have been questioned when one moves to much more complex systems, such as the whole brain [12]. As of today, the only means to directly record the electric activity of the brain in vivo and noninvasively are electroencephalogram (EEG) and magnetoencephalogram (MEG) [13]. The features of those signals have been exploited in order to measure synchronization between functional brain areas. A number of metrics have been designed in order to quantify synchronization between areas [4]. When estimating connectivity using such metrics, one main problem stems from the fact that each source activity is simultaneously recorded by multiple sensors [14], [15]. This phenomena, commonly referred to as volume conduction or field spread, can result in the presence of spurious linear correlations that negatively affects estimation of the statistical dependencies between time series. To this regard, Nolte et. al proposed the imaginary part of coherence (ImC) as a way to overcome this limitation [16].

Manuscript received July 20, 2018; revised September 21, 2018; accepted September 27, 2018. Date of publication November 5, 2018; date of current version April 2, 2019. *(Corresponding author: Fabio Baselice.)*

F. Baselice and A. Sorriso are with the Department of Engineering, University of Naples Parthenope, 80143 Naples, Italy (e-mail: fabio.baselice@uniparthenope.it; antonietta.sorriso@uniparthenope.it).

R. Rucco is with the Department of Motor Sciences and Wellness, University of Naples Parthenope, 80133 Naples, Italy, also with the Hermitage-Capodimonte Hospital, 80131 Naples, Italy, and also with the Institute of Applied Sciences and Intelligent Systems, CNR, 80078 Pozzuoli, Italy (e-mail: rosaria.rucco@uniparthenope.it).

P. Sorrentino is with the Department of Engineering, University of Naples Parthenope, 80143 Naples, Italy, also with the Hermitage-Capodimonte Hospital, 80131 Naples, Italy, and also with the Institute of Applied Sciences and Intelligent Systems, CNR, 80078 Pozzuoli, Italy (e-mail: pierpaolo.sorrentino@uniparthenope.it).

Color versions of one or more of the figures in this paper are available online at http://ieeexplore.ieee.org.

Digital Object Identifier 10.1109/TMI.2018.2873423

The reasoning behind this is that the same source would affect two time series without time delay, hence their cross-spectrum in zero would have null imaginary part. However, the ImC depends also upon the amplitude of the signal, and so it cannot be considered as a pure phase-based metric [17]. In order to design a pure phase based metric while preserving the insensitivity to volume conduction, Stam et al. proposed the Phase Lag Index (PLI) [17]. The PLI is computed as the time average of the signum of the phase differences between the series. It is based on the concept that two synchronized time sources will show a constant phase difference over time. The PLI is insensitive to volume conduction while remaining a pure phase-based metric. However, the PLI has shown to be rather sensitive to noise, an issue particularly relevant in the case of signals received with small delays, which are known to be abundant in the brain [18], [19]. The sensitivity to noise of the PLI led to the introduction of the weighted PLI (wPLI), whereby the PLI is multiplied by the imaginary part of the cross-spectrum [20]. Values derived from signals with small phase differences (i.e. with a small imaginary part), that are more likely to be affected by noise, will contribute less to the final estimate. Unfortunately, the weighting procedure introduces again a dependency upon the amplitude, therefore such metric carries slightly different information and is to be interpreted differently from the PLI and the PLM. Hence, when the estimation of communication is based solely on the phase, sensitivity to noise becomes crucial, hindering the possibility of reliably estimating brain connectivity at the single subject level [18]. In order to achieve a metric that is purely phase-based, while being resilient to noise and informative about synchronization, one should remember that, even in the early works (both theoretical or on simple models), the dynamic of synchronization changed significantly if the characteristics of the oscillators were allowed to vary (which seems a reasonable assumption when dealing with complex systems, such as the human brain [12]). One (of many) important examples of this was shown by Winfree [11], who showed that, if the frequencies of the oscillators are allowed to differ within a range, synchronization can still occur.

In this manuscript, we introduce a new phase-based metric, that we named the Phase Linearity Measurement (PLM), designed to be robust to noise and insensitive to volume conduction. The PLM, similarly to the PLI, is interpretable when dealing with narrow-band signals, as it exploits the phase differences between them. The novelty of such metric consists in the fact that a small band of frequencies is considered relevant in establishing communication between functional brain areas. To this regard, the PLM differs from the PLI, that only takes into account the components in perfect iso-frequency when estimating synchronization. This is to say that the PLM measures linear trends of the differential phase instead of constant ones. Therefore, the PLM could be thought of as an extension of the PLI, aiming at measuring the similarity of phase behaviors between signals. In order to achieve such result, the metric exploits the relative energy carried by phasors composing the cross-spectrum of two signals. While being a pure phase-based metric, the PLM cannot be considered as a classical measure of synchronization, given that it measures the dependency between signals even if their phase differences are not constant over time (indeed the PLM will detect if those values evolve linearly over time).

In this work, the PLM is analytically presented in Section II. Following that, we tested the ability of the PLM to measure coupling. In order to do so, we have generated a series of coupled Rössler attractors with varying degree of synchronization, and compared the performance of the PLI and the PLM in detecting coupling. Following this step, we have corrupted such time series with growing levels of noise, and compared the robustness of the PLI and the PLM against noise. Then, a model based on Gaussian realizations of a random variable, with varying degrees of correlation between the signals, has been considered. Furthermore, we have introduced varying degrees of (small) differences in the central resonance frequency of the signals. Then, the performances of the PLI and the PLM have been compared, both with and without noise. In order to validate our approach on real data, a MEG dataset has also been analyzed. The connectivity matrices obtained using the PLM, the PLI and the Amplitude Envelope Correlation (AEC) [21] have been compared, and the robustness of the metrics with respect to noise has been measured. The AEC has been considered, despite not being a phase-based metric, given its very good properties of robustness against noise [22]. Results are encouraging and, most importantly, the PLM reaches stability and optimal Signal to Noise Ratio (SNR) with averaging over only a few epochs, allowing a reliable measurement of the connectivity at the single subject level.

## II. Methods

Let us consider two real signals $s_1(t)$ and $s_2(t)$. The corresponding analytical signals are defined as:

$$\begin{aligned} x(t) &= s_1(t) + i\tilde{s}_1(t) = A_x(t)e^{i\phi_x(t)} \\ y(t) &= s_2(t) + i\tilde{s}_2(t) = A_y(t)e^{i\phi_y(t)} \end{aligned} \tag{1}$$

where $\tilde{s}(t)$ is the Hilbert transform of the signal $s(t)$, i.e.:

$$\tilde{s}(t) = \frac{1}{\pi} PV \int_{-\infty}^{\infty} \frac{s(\tau)}{t-\tau} \mathrm{d}\tau \tag{2}$$

with $PV$ the Cauchy principal value. Starting from the analytical signals, let us define the *interferometric* signal $z(t)$ as:

$$z(t) = x(t)y'(t) \tag{3}$$

where the symbol $'$ indicates the complex conjugate. Moving to the modulus and phase notation, such signal can be expressed as:

$$z(t) = A_x(t)A_y(t)e^{i[\phi_x(t)-\phi_y(t)]} = A_x(t)A_y(t)e^{i[\Delta\phi(t)]} \tag{4}$$

In brief, the amplitude of $z(t)$ is the product of the amplitudes of $x(t)$ and $y(t)$, while the phase is their phase difference $\Delta\phi(t) = \phi_x(t) - \phi_y(t)$. Note that, by applying the normalization and the temporal mean operator $\langle\cdot\rangle$ to $z(t)$, the complex coherence value $c$ of the two signals is computed:

$$c = \frac{\langle z(t)\rangle}{\sqrt{\langle A_x^2(t)\rangle\langle A_y^2(t)\rangle}} \tag{5}$$

In order to remove the contribution of the linear mixing of uncorrelated sources, i.e. the volume conduction, from the connectivity measurement, it has been proposed in [16] to only consider the imaginary part of $c$:

$$\Im\{c\} = \frac{\langle A_x(t)A_y(t)\sin[\Delta\phi(t)]\rangle}{\sqrt{\langle A_x^2(t)\rangle\langle A_y^2(t)\rangle}} \tag{6}$$

where the sin function makes the fraction null in case of $\Delta\phi = 0$. Another well established functional connectivity measurement (practically) unaffected by the volume conduction is the PLI, which analyses the sign of the $\Delta\phi(t)$ term:

$$\text{PLI} = |\langle \text{sgn}[\Delta\phi(t)]\rangle| = |\langle \text{sgn}[\angle z(t)]\rangle| \tag{7}$$

where the operator $\angle\cdot$ extracts the phase of the signal. The idea is that, in case of two correlated sources, the phase difference remains constant over time (disregarding the noise), i.e. $\Delta\phi(t) = \Delta\phi$. More in detail, if the two sources share the same frequency behavior $f_x(t) = f_y(t) = f_0(t)$, their phases can be written as (we assume the signals start at $t = 0$):

$$\begin{aligned}\phi_x(t) &= \int_0^t f_0(\tau)\mathrm{d}\tau + \varphi_x \\ \phi_y(t) &= \int_0^t f_0(\tau)\mathrm{d}\tau + \varphi_y\end{aligned} \tag{8}$$

with $\varphi_x$ and $\varphi_y$ the initial phases related to signal propagation delays. In this case, the phase difference $\Delta\phi(t)$ is constant:

$$\Delta\phi(t) = \phi_x(t) - \phi_y(t) = \varphi_x - \varphi_y \tag{9}$$

If the instantaneous frequencies of the two signals $s_1(t)$ and $s_2(t)$ are not exactly the same over time, but show a constant difference, defined as $\Delta f$, i.e. $f_x(t) = f_0(t)$ and $f_y(t) = f_0(t) + \Delta f$, the phase difference will no longer be characterized by a constant behavior. Eq. (8) and (9) are thus modified in:

$$\begin{aligned}\phi_x(t) &= \int_0^t f_0(\tau)d\tau + \varphi_x \\ \phi_y(t) &= \int_0^t f_0(\tau)d\tau + \Delta f t + \varphi_y\end{aligned} \tag{10}$$

and

$$\Delta\phi(t) = \phi_x(t) - \phi_y(t) = \varphi_x - \varphi_y - \Delta f t \tag{11}$$

Note that the above equation describes the behavior of the phase difference term as linear over time, which is different from Eq. (9), where $\Delta\phi(t)$ is constant. The PLI has a serious limitation in this specific case, as it has been designed under the hypothesis of Eq. (9) instead of Eq. (11). More in detail, a $\Delta\phi(t)$ variation equal to $\pi/2$ within the observation interval $T$ is sufficient to greatly reduce the measured PLI value. It is worth to underline that this effect happens also in case of very limited $\Delta f$ values. For example, assuming $T = 10$s, this effect appears for $\Delta f \geqslant 0.025$ Hz.

Within this work, a novel functional connectivity index able to handle narrow $\Delta f$ values is proposed. The index, which has been named Phase Linearity Measurement (PLM), can be seen as a generalization of the PLI, as developed considering Eq. (11) as the differential phase model. Let us consider the interferometric signal $z(t)$ of Eq. (4). The first step consists in setting the amplitude equal to 1 in order to remove its effect, leading to a normalized $z(t)$:

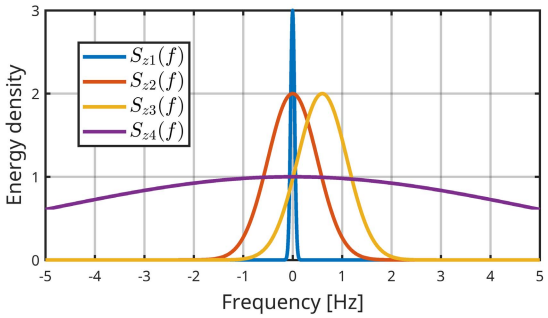


Fig. 1. Four energy spectral densities of the interferometric signal $z(t)$ case of iso-frequency and high correlation ($S_{z1}(f)$), iso-frequency and medium correlation ($S_{z2}(f)$), non iso-frequency and medium correlation ($S_{z3}(f)$) and low correlation ($S_{z4}(f)$) signals. In $S_{z3}(f)$ PLM detects connectivity, unlike PLI.

$$z_N(t) = e^{i\angle z(t)} = e^{i\Delta\phi(t)} \tag{12}$$

The PLM reveals the presence of phase variations of the 0-th order (i.e. the term $\varphi_x - \varphi_y$, which is constant) and of the 1-st order (i.e. the linear term $\Delta f t$) within the normalized interferometric signal $z_N(t)$. In other words, the analysis consists in decomposing the normalized interferometric signal of Eq. (12) into a set of phasors at fixed frequencies, and evaluating their relative energies. Such evaluation can be effectively performed via the direct Fourier transform of $z_N(t)$:

$$Z_N(f) = \int_0^T z_N(t)e^{-i2\pi ft}\mathrm{d}t \tag{13}$$

where $[0,\ T]$ is the signals observation period. By computing the energy spectral density

$$S_z(f) = |Z_N(f)|^2, \tag{14}$$

the predominant frequency components of $z_N(t)$ can be identified. It has to be underlined that the band of $S_z(f)$ is not directly related to the frequency bands of the original signals $x(t)$ and $y(t)$, but rather on the shape of their cross-correlation function. In Figure 1, four different energy spectral densities are reported. $S_{z1}(f)$ (blue line) is characterized by an energy peak around $f = 0$ Hz, and it is related to highly correlated sources (highest peak value) with the same frequency, i.e. $\Delta\phi(t) = \Delta\phi$ (constant phase difference). In this case, the PLI is an effective connectivity measurement. The function $S_{z2}(f)$ (orange line) is similar, but the energy is distributed on a wider frequency range (about $[-1,\ 1]$ Hz in the example). This condition is related to two sources characterized by lower correlation with respect to the previous case, but again the same frequency behavior. The PLI provides a valid measurement also in this case. The third spectral density $S_{z3}(f)$ (yellow line) shows the same correlation value of $S_{z2}(f)$ (same peak height), but a frequency shift appears between the two signals as revealed by the shift of the peak (specifically $\Delta f = 0.6$ Hz). The $S_{z4}(f)$ spectrum (violet line) is related to uncorrelated sources (lower peak height) and shows a characteristic wide-band behavior. In case of $S_{z3}(f)$ and $S_{z4}(f)$, the PLI measures

very low connectivity, but this is true only for the latter. The aim of the PLM is to measure the connectivity of $S_{z3}(f)$ in a correct way, i.e. properly handling frequency shifts between signals. The PLM is defined by the following equation:

$$\text{PLM} = \frac{\int_{-B}^{B} S_z(f)\mathrm{d}f}{\int_{-\infty}^{\infty} S_z(f)\mathrm{d}f} \tag{15}$$

In brief, the PLM computes the percentage of the spectral energy within a narrow band $2B$ centered around 0 with respect to the total energy of the signal. By looking at the spectra reported in Figure 1, it is evident that the PLM is capable of correctly measuring the correlation, producing a high value in case of $S_{z1}(f)$, $S_{z2}(f)$ and $S_{z3}(f)$ and a low value in case of $S_{z4}(f)$ (its energy spreads over a wide range of frequencies). By merging Eqn. (12), (13) and (15), the PLM can be defined as:

$$\text{PLM} = \frac{\int_{-B}^{B} |\int_{0}^{T} e^{i\Delta\phi(t)} e^{-i2\pi f t}\mathrm{d}t|^2 \mathrm{d}f}{\int_{-\infty}^{\infty} |\int_{0}^{T} e^{i\Delta\phi(t)} e^{-i2\pi f t}\mathrm{d}t|^2 \mathrm{d}f} \tag{16}$$

Of course, in case of numeric data the Fast Fourier Transform algorithm can be exploited for efficiently computing Eq. (16).[1]

*Volume Conduction Effect:* Within this subsection the effects of the Volume Conduction (VC) artifact on the PLM are investigated [23]. Let us focus on the complex Fourier transform of the interferometric signal defined in Eq. (13). In case of two iso-frequency signals, $Z_N(f)$ will have the maximum amplitude value at $f = 0$ Hz, and a phase value related to the delay between the two signals. Such phase value can be analyzed in order to detect VC artifacts. In particular, the VC effect is instantaneous, thus it is characterized by a very small phase difference (close to zero). Therefore, before computing the energy spectral density $S_z(f)$, the amplitude of $Z_N(f)$ at $f = 0$ is set equal to zero in case its phase value is below the threshold $\varepsilon$, i.e:

$$Z_N(0) = \begin{cases} 0 & \text{if } |\angle Z_N(0)| < \varepsilon \\ Z_N(0) & \text{if } |\angle Z_N(0)| \geq \varepsilon \end{cases} \tag{17}$$

Appropriate values of $\varepsilon$ mainly depends on the noise level. An analysis has been carried out in Section III. By applying Eq. (17) before computing the energy spectral density $S_z(f)$, the contribution of the VC to the PLM is eliminated.

## III. Results

### A. Choice of the Integration Band

In order to set the integration band $B$, we based our analysis on real data. More in detail, two couples of sources have been selected, with the highest and lowest connectivity values. The PLM has been computed varying $B$ between 0.1 and 5 Hz. Means and normalized standard deviations are reported in Figure 2. It can be noticed that the distance between the mean values is maximized when $B$ is close to 1 Hz, and that the wider the integration band, the lower the standard deviation. Given such results, for all the analysis, we set $B = 1$ Hz.

[1]The PLM code is available in the Fieltrip toolbox and upon request.

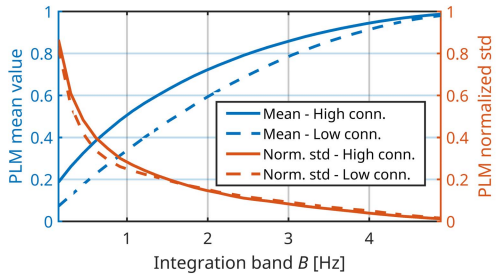


Fig. 2. Mean values (blue lines) and normalized (over mean) standard deviations (orange lines) of PLM in case of high (solid lines) and low (dashed lines) connectivity as a function of the integration band $B$.

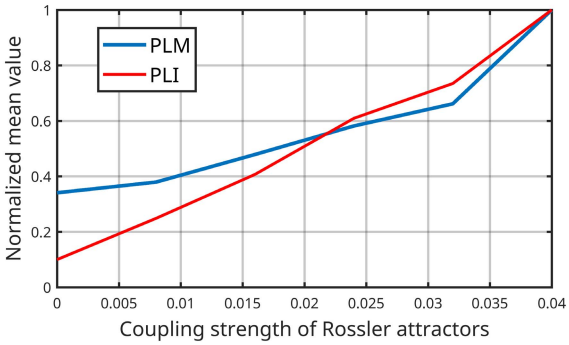


Fig. 3. Mean values of PLM (blue) and PLI (red) in Rössler oscillators as a function of coupling strength, from 0 (no coupling) to 0.04 (high coupling). Both metrics grow monotonically as a function of connectedness.

### B. Simulated Data - Rössler Oscillator

In this Section, an analysis on the effectiveness of the PLM in measuring synchronization has been carried out, together with its robustness against noise. We chose the Rössler oscillators to model neuron ensembles and generate datasets with different level of synchronization. In particular, the time series have been generated according to [24] with coupling strength varying between 0 and 0.04. The duration and the sampling interval have been set equal to 5000 s and $2\pi \cdot 10^{-4}$ s, respectively. Both the PLM and the PLI have been computed, producing the results showed in Figure 3, where the normalized measured values have been reported. For this analysis, and for all those reported in the following ones, we considered $B = 1$ Hz.

The two Rössler oscillators with the same characteristics have also been implemented for the noise robustness analysis. In this case, white Gaussian noise has been added to the data, and Monte Carlo simulations with $10^3$ realizations have been set up in order to evaluate the normalized standard deviations (i.e. the standard deviation over the mean value) of the PLM and the PLI in case of SNR equal to 10 dB (high noise), 20 dB (medium noise) and 30 dB (low noise). Results are reported in Figure 4.

An analysis of proper values of the threshold $\varepsilon$ of Eq. (17) is now conducted. Two iso-frequency coupled signals have been generated in the alpha band with the same phase ($\Delta\phi(t) = 0$). Noise has been added in order to achieve SNR values between 10 and 30 dB. Subsequently, the interferometric signal in the

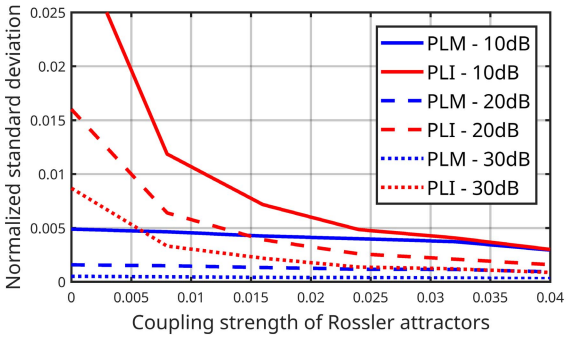


Fig. 4. Normalized (over mean) standard deviations of PLM (blue) and PLI (red) in Rössler oscillators as a function of coupling strength, in case of SNR equal to 10 dB (solid lines), 20 dB (dashed lines) and 30 dB (dotted lines). PLM has good resiliency to noise.

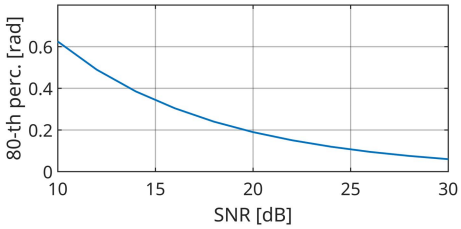


Fig. 5. 80-th percentile values of the interferometric phase in case of different SNRs. The lower the noise, the smaller the phase (in case of $f = 0$).

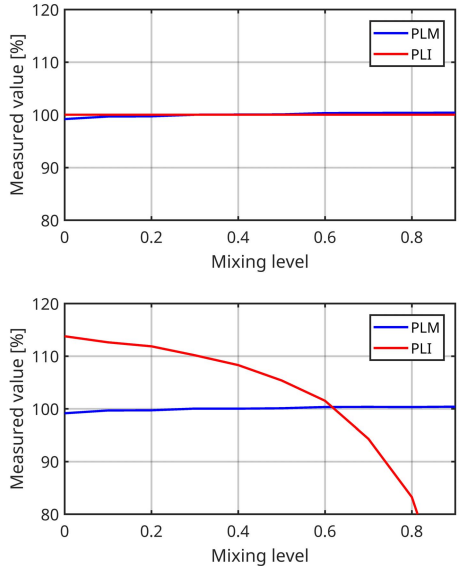


Fig. 6. PLM (blue) and PLI (red) measured values for different mixing levels in case of no noise (top) and *SNR* = 30dB (bottom). The PLM remains steady despite noise.

frequency domain $Z_N(f)$ is computed, and the phase values at $f = 0$ are analyzed. More in detail, the statistical distribution is empirically estimated and the 80-th percentile value is extracted at different noise levels (Figure 5). For example, in case of data with SNR = 30dB, an $\varepsilon$ value of 0.05 rad (about 2.8°) will allow to reject 80% of the components related to the VC. Such values, which depends on the SNR, should be set within Eq. (17) in order to properly avoid the influence of the VC over the coupling measure.

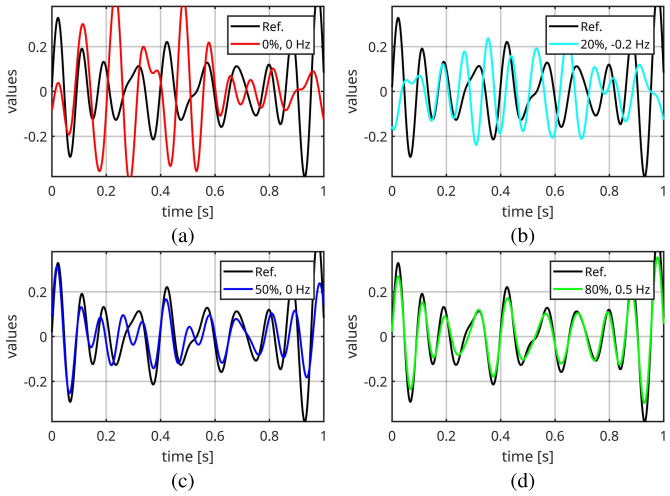


Fig. 7. Signals simulated over time (1s): uncorrelated ($\rho = 0$) (a), small correlation non iso-frequency ($\rho = 0.2$, $_1f = -0.2$ Hz) (c), medium correlation iso-frequency ($\rho = 0.5$, $_1f = 0$ Hz) (c), high correlation, non iso-frequency ($\rho = 0.8$, $_1f = 0.5$ Hz) (d) and reference signal (red lines).

In order to test the effects of the volume conduction, a further simulation is implemented. Following the approach reported in [25], signals related to two Rössler oscillators with coupling coefficient $c = 0.04$, namely $r_1(t)$ and $r_2(t)$, are generated and linearly mixed according to:

$$x(t) = \left(1 - \frac{m}{2}\right) r_1(t) + \frac{m}{2} r_2(t)$$
$$y(t) = \frac{m}{2} r_1(t) + \left(1 - \frac{m}{2}\right) r_2(t) \qquad (18)$$

where the variable $m$ controls the linear mixing strength. In particular, the condition $m = 0$ refers to the no volume conduction case, while the two signals are perfectly linearly mixed ($x(t) = y(t)$) in case of $m = 1$. A Monte Carlo simulation has been conducted for testing the performances of the PLM, and comparing them to the PLI, in case of $m$ varying from 0 to 1. Results are reported in Figure 6.

### C. Simulated Data - Gaussian Process

A Monte Carlo simulation has been set up in order to validate the proposed methodology in case of non-isofrequency signals. In order to to this, $10^3$ realizations (epochs) of 5 white Gaussian processes with zero mean and unitary variance have been generated. Each process has been sampled at 625 Hz for 6.5 seconds, collecting 4096 time samples. A bandpass filter in the range [7, 13] Hz has then been applied. Subsequently, correlations ($\rho_{25} = 0.2$, $\rho_{35} = 0.5$ and $\rho_{45} = 0.8$) and frequency shifts ($\Delta f_{25} = -0.2$ Hz and $\Delta f_{45} = +0.5$ Hz) have been applied to the data. Moreover, in order to avoid zero phase difference (i.e. VC effect), a constant phase shift (equal to $\pi/10$ radiants) has been added to the reference signal. One second of the generated signals is reported in Figure 7: the black lines are the reference signals, the red line is the uncorrelated signal in Figure 7(a)), and the cyan, blue and green lines of Figures 7(b-d) represent signals with different correlation levels (20%, 50% and 80%, respectively) and frequency shifts (−0.2Hz, 0Hz and 0.5Hz, respectively)

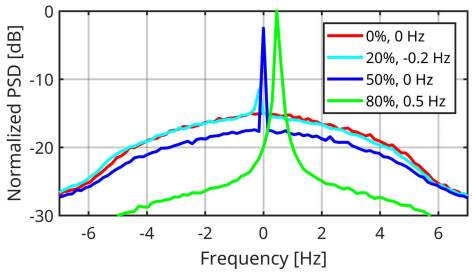


Fig. 8. Power spectral densities of the simulated interferometric signals couples in the range $[-4, 4]$ Hz and in logarithmic scale: uncorrelated case ($\rho = 0$) (red line), small correlation, non iso-frequency ($\rho = 0.2$, $\Delta f = -0.2$ Hz) (cyan line), medium correlation, iso-frequency ($\rho = 0.5$, $\Delta f = 0$ Hz) (blue line), high correlation, non iso-frequency ($\rho = 0.8$, $\Delta f = 0.5$ Hz) (green line). Peak intensities and positions are in accordance with correlations and frequency shifts among considered signals.

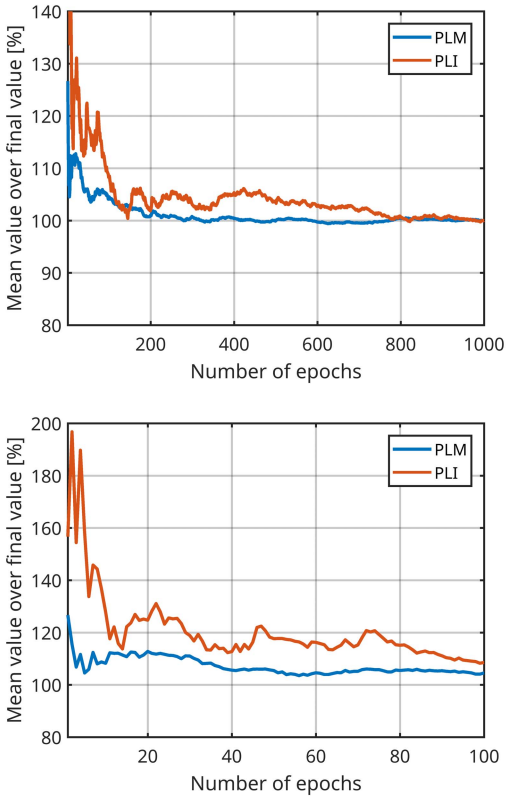


Fig. 9. PLM (blue line) and PLI (red line) values averaged over 1 to 1000 epochs (top), and an enlargement over the first 100 epochs (bottom). The two indexes converge to 100% of their final value with different speed.

as compared to the reference signal. The interferometric signals have been computed with respect to the reference one both in the time and the frequency domains, according to Eqn. (3) and (13). Subsequently, the power spectral densities $S_z(f)$ have been computed and reported in Figure 8. As expected, the curve of the uncorrelated case (blue line) spreads over the considered frequency range, while the other behaviors are characterized by power peaks with different intensities (related to the correlation value) and positions (related to the frequency shifts).

The signals generated within the Monte Carlo simulation have been corrupted by an additive zero mean white Gaussian

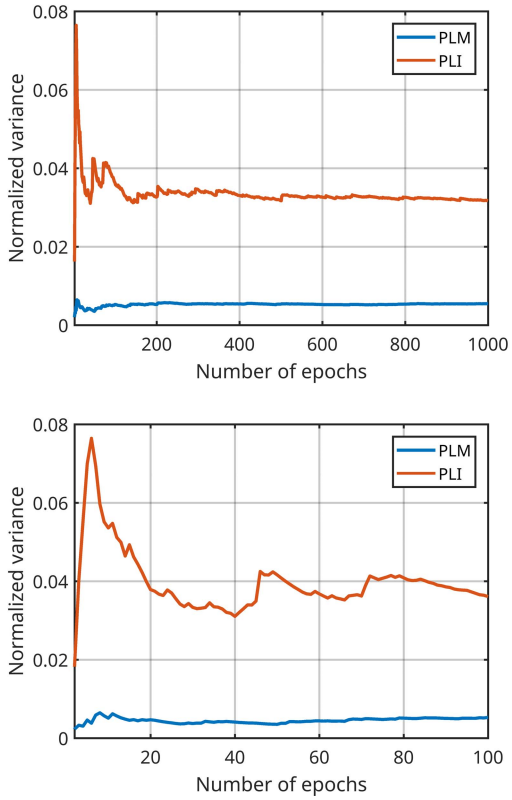


Fig. 10. PLM (blue line) and PLI (red line) normalized variances computed over 2 to 1000 epochs (top), and an enlargement over the first 100 epochs (bottom).

noise in order to reach an SNR of 20 dB. The PLM and the PLI have been computed for all the realizations of the Monte Carlo simulation. Their mean and variance values have been computed varying the number of epochs up to $10^3$, according to:

$$\mu_{PLI}(k) = 100\frac{1}{\mu_{PLI}(mc)}\frac{1}{k}\sum_{i=1}^{k} PLI(i)$$

$$\mu_{PLM}(k) = 100\frac{1}{\mu_{PLM}(mc)}\frac{1}{k}\sum_{i=1}^{k} PLM(i)$$

$$\sigma^2_{PLI}(k) = \frac{1}{\mu_{PLI}(mc)}\frac{1}{k-1}\sum_{i=1}^{k}[PLI(i) - \mu_{PLI}(k)]^2$$

$$\sigma^2_{PLM}(k) = \frac{1}{\mu_{PLM}(mc)}\frac{1}{k-1}\sum_{i=1}^{k}[PLM(i) - \mu_{PLM}(k)]^2$$

with $k = 1, \ldots, mc$, where $mc$ is the Monte Carlo number, $PLI(i)$ and $PLM(i)$ refer to the indexes computed in case of the $i$-th epoch. The behaviors of mean and variance are reported in Figures 9 and 10.

Another Monte Carlo simulation has been set up in order to evaluate the performances of the PLM and the PLI when a varying number of epochs is averaged. In particular, we compared the mean values of the PLI and the PLM computed averaging a number of epochs varying between 1 and 200. For each number of epochs, $10^4$ Monte Carlo realizations

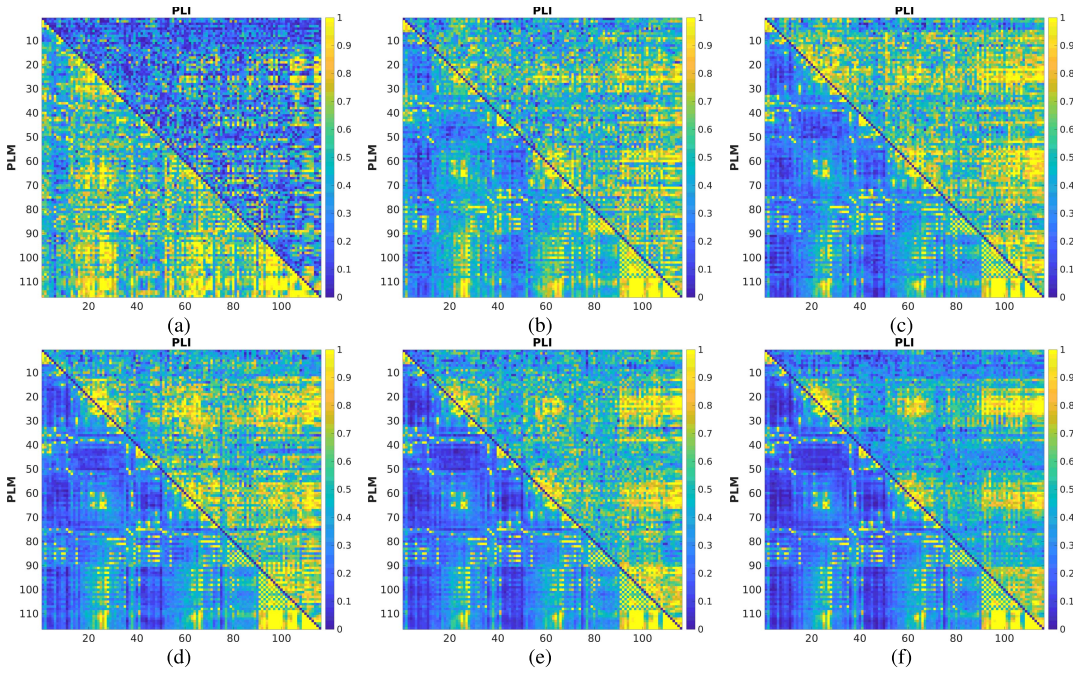


Fig. 11. Comparison between PLI (upper triangular) and PLM (lower triangular) indexes in case of 1 (a), 10 (b), 30 (c), 50 (d), 100 (e) and 200 (f) epochs of an heterogeneous population. PLM converges faster than PLI. All epochs are 8 s long.

TABLE I
NORMALIZED STANDARD DEVIATIONS OF THE PLI AND THE PLM WHEN AVERAGING OVER DIFFERENT NUMBER OF EPOCHS

| | 1 ep. | 5 ep. | 10 ep. | 20 ep. | 50 ep. | 100 ep. | 200 ep. |
|---|---|---|---|---|---|---|---|
| PLI | 0.757 | 0.336 | 0.240 | 0.167 | 0.106 | 0.075 | 0.054 |
| PLM | 0.247 | 0.109 | 0.078 | 0.055 | 0.035 | 0.025 | 0.017 |

have been generated in order to achieve effective estimations. In Table I, the normalized standard deviations (i.e. divided by the mean) are reported.

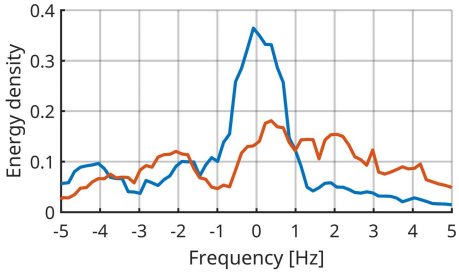


Fig. 12. Power spectral densities of two interferometric signals related to a pair of coupled (blue line) and uncoupled (red line) sources. The analysis is related to the alpha band.

### *D. Real Data*

In order to record the magnetic fields produced by the brain, we used a magnetoencephalographic (MEG) system developed by the Institute of Applied Sciences and Intelligent Systems of the Italian National Research Council (CNR) [26]. The 47 subjects were seated inside a magnetically shielded room (AtB Biomag UG - Ulm - Germany) and spontaneous brain activity was recorded in a five minute, no task, eyes closed condition. The data was sampled at 1024 Hz and band-pass filtered within the range [0.5, 100] Hz. Principal Component Analysis (PCA) was performed using the reference sensors in order to reduce the environmental noise [27]. Noisy channels were removed manually through visual inspection, while the ECG components were removed from the data using supervised Independent Component Analysis (ICA) [28]. Subsequently, signals have been resampled at 512 Hz and filtered within the alpha band [7, 13] Hz. Epochs of 8 s (4096 samples) have been extracted. Such epoch length has been chosen in order to obtain a reliable and stable estimate of the PLI [29]. Epochs that did not contain artifacts (either system related or physiological) or excessive environmental noise were selected manually by an experienced rater, and overall roughly 500 epochs were available in the sensor space.

Fieldtrip Toolbox [30] in Matlab$^{TM}$ environment has been used for the beamforming operation. In particular, the Linear Constraint Minimum Variance algorithm [31] was adopted, based on the native MRI of the subjects and on the 116 areas of interest according to the AAL atlas, each one corresponding to a neurologically meaningful anatomical area [32].

Firstly, based on the PLI, we selected the most and the least connected couples of sources and computed their interferometric signals $z_N(t)$. For both of them, the frequency spectra $S_z(f)$ have been computed and reported in Figure 12. The red line in Figure 12 corresponds to the violet line in Figure 1, both related to uncoupled signals. Similarly, the blue line in Figure 12 and the red line in Figure 1 correspond to the coupled signals.

The PLM has been compared to the PLI [17] and to the AEC [21], which extracts signal envelopes and measures the coupling by computing their correlation, varying the number

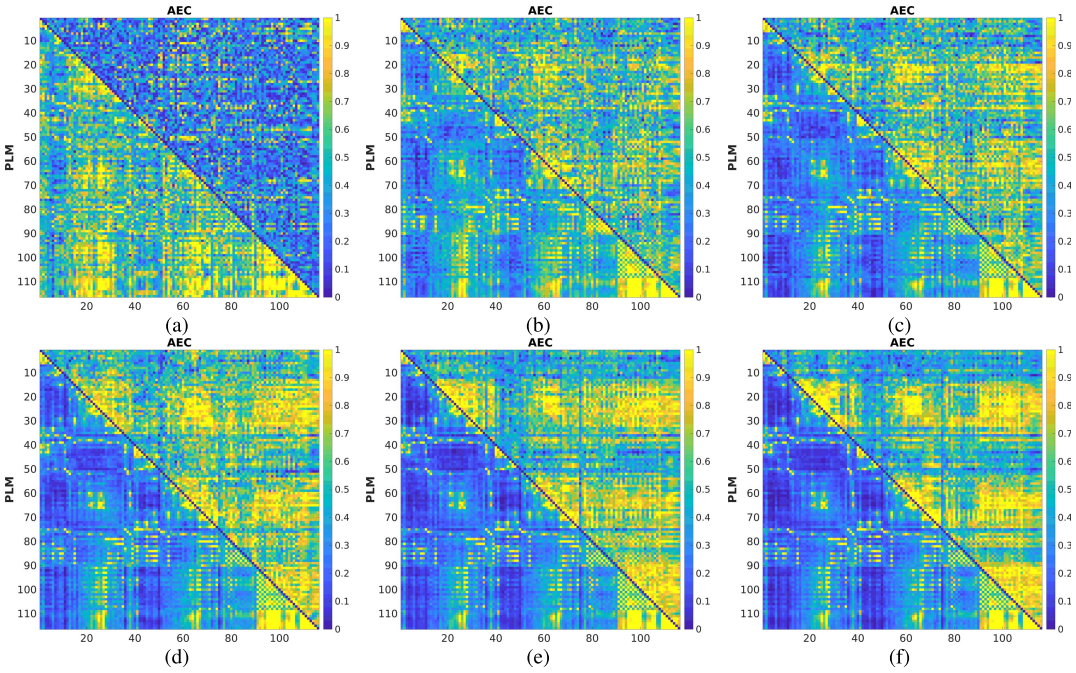


Fig. 13. Comparison between AEC (upper triangular) and PLM (lower triangular) indexes in case of 1 (a), 10 (b), 30 (c), 50 (d), 100 (e) and 200 (f) epochs of an heterogeneous population. PLM converges faster than AEC. All epochs are 8 s long.

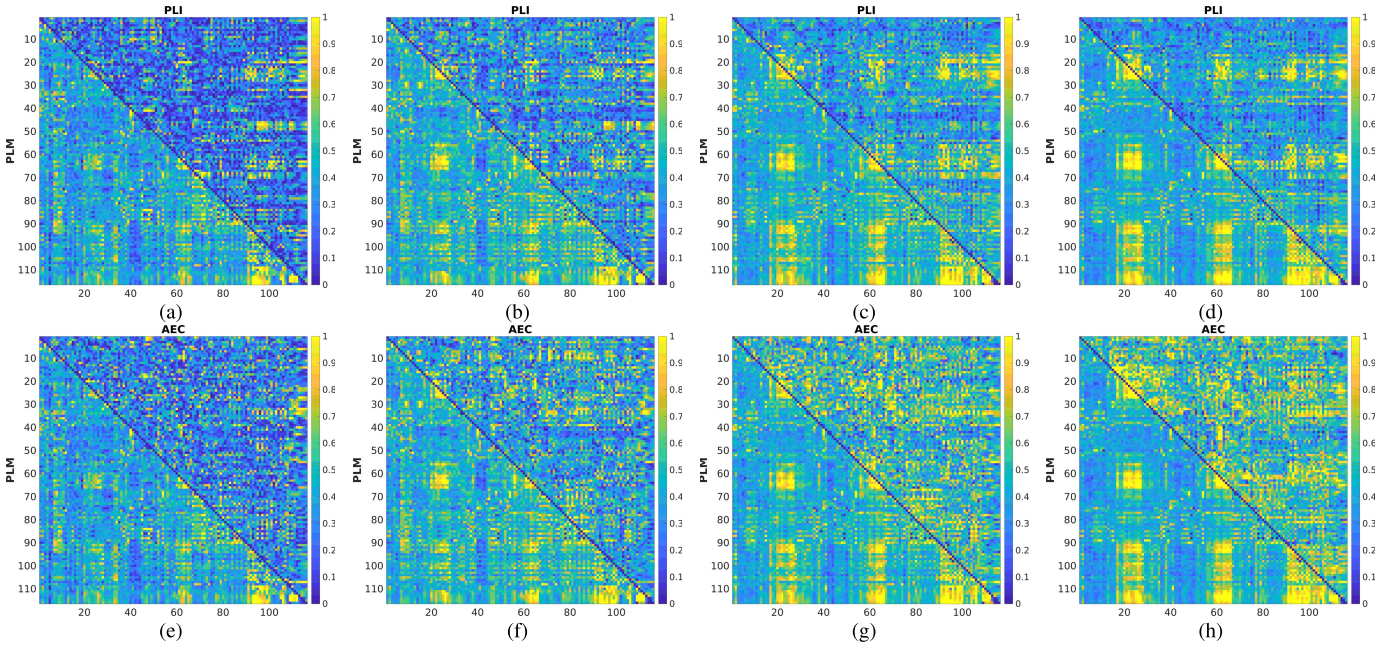


Fig. 14. First row: comparison between PLI (upper triangular) and PLM (lower triangular) indexes. Second row: comparison between AEC (upper triangular) and PLM (lower triangular) indexes. Results refer to the case of 1 (a,e), 2 (b,f), 5 (c,g) and 10 (d,h) epochs of a single subject. All epochs are 8 s long.

of epochs. The comparison between the PLM and the PLI is reported in Figure 11. The matrices have been computed and averaged varying the number of epochs. More in details, Figure 11(a) shows the upper (PLI) and lower (PLM) triangular matrix computed on a single epoch, while Figures 11(b)-(f) refer to the average over 10, 30, 50, 100 and 200 epochs, respectively. Similarly, the PLM is compared to the AEC in Figure 13. The comparisons of the PLM with the PLI and the AEC have also been done in the case of a single subject in order to remove the intra-population variability. The considered indexes have been computed varying the number of epochs between 1 and 10. Results are reported in Fig. 14.

A last analysis has been conducted by comparing PLM and PLI connectivity matrices averaged over 50 epochs to the result obtained averaging 200 epochs. The analysis has been repeated 1000 times, each one with a different permutation of the initial data. For each permutation, the relative mean square difference between the two matrices (i.e. 50 and 200 epochs)

has been computed. In order to statistically compare the two indexes, the Wilcoxon signed rank test has been adopted. Such test confirms that the PLM is statistically significantly faster in reaching convergence than the PLI ($p$-value $< 10^{-160}$).

## IV. Discussion

Within this manuscript, a novel methodology for measuring brain functional connectivity has been presented. We named it Phase Linearity Measurement (PLM). The PLM provides an adirectional estimate of the connectivity that is purely based upon the phases of the signals. Overall, the idea behind the PLM is that two sources that are communicating will produce signals with a phase difference evolving linearly over time. The slope of this linear behavior will be dependent upon the difference in the central frequency of the two signals. With the PLM, we aimed at using this feature in order to obtain a metric that is purely phase dependent and that is robust enough with respect to noise to be used at the single-subject level.

By looking at the results of the simulations with Rössler oscillators (Figure 3), it is evident that both the PLM and the PLI measure the synchronization, producing a monotonically increasing function directly related to the coupling strength.

The sensitivity to noise of the PLM, in comparison to that of the PLI, in case of different noise levels and coupling strengths can be appreciated in Figure 4. From the graphs, it is evident that the PLM (blue curves) produces more stable results, i.e. lower standard deviation, with respect to the PLI in all the considered cases. In particular, the difference is remarkable in case of very low coupling strengths and high SNR (Fig. 4).

Figure 6 shows that PLM is insensitive to volume conduction effect. More in detail, in case of no noise (Figure 6, top) the measured PLM values show a variation below 1%, while the PLI shows no significant variation. In case of noise (SNR = 30 dB), reported in Figure 6, bottom, PLM confirms such behavior, while the PLI performances are deeply affected.

Moving to the non iso-frequency case, modeled by a Gaussian process, the PLM is more robust to noise as compared to the PLI (Figures 9 and 10). In fact, in case of SNR = 20dB, the PLM reaches the [90%, 110%] interval in less than 20 epochs, as compared to the PLI, that requires more than 100 epochs. The normalized variance curves confirm such finding. In particular, the normalized variance in case of $k = 10^3$ epochs is about 0.005 for the PLM and 0.03 for the PLI. The performances of the PLM and the PLI in case of different epoch number are reported in Table I. In the case of only one epoch, the PLI value has a standard deviation of about 76% of its mean value, while the PLM gives a much more reliable estimation (standard deviation below 25%). As expected, if more epochs are available, both the PLI and the PLM become more reliable. In particular, computing the PLI and the PLM by averaging 100 epochs makes their normalized standard deviations equal to 7% and 2%, respectively. From the values reported in Table I, it can be stated that the standard deviation of the PLM is three times lower than that of the PLI.

This peculiarity appears also using real data. The real data we used for testing are obtained from a MEG device located in a hospital, producing signals in a realistic environment and with a significant level of noise. In order to test robustness against noise, we studied how many epochs are needed to reach a reliable estimate of the connectivity matrix in the alpha band. Such information is also useful in order to understand if the PLM is a good candidate to move from the group level to the individual level analysis. As expected from the simulated data, the robustness to noise of the PLM can be easily appreciated, as compared to the PLI. In particular, in the case of the PLM, 30 epochs suffice to produce a matrix similar to the one obtained averaging 200 epochs. In the case of PLI, much more data are needed to obtain such result.

Moving to the comparison between the PLM and the AEC (Figure 13), one can appreciate that the AEC, similarly to the PLI, requires much more data in order to provide reliable results than the PLM.

The comparisons of the PLM with the PLI and the AEC have also been done in the case of a single subject in order to remove the intra-population variability. The considered indexes have been computed varying the number of epochs between 1 and 10. The results, reported in Figure 14, confirm the previous findings. Both the PLI and the AEC require much more data than PLM for providing reliable results. Therefore, the PLM bears promise to the possibility of estimating connectivity at the single subject level.

Furthermore, when a small difference between the frequencies of the two generated signals is present, the PLI loses its ability to detect coupling. The PLI has been designed in such a way based upon the definition of synchronization between two signals by assuming an almost constant value of the phase difference over time. To this regard, it makes sense that the PLI would be zero in case of a shift between the frequencies of the signals, since the evolution of the phase differences would follow a linear trend, instead of a constant one, hence assuming all possible values in the $]-\pi, \pi]$ range. However, here we assume that two oscillators are coupled even if their intrinsic features differ slightly, hence when their phase difference evolves linearly over time. According to this hypothesis, the PLM has been designed to measure coupling even in the case of small frequency differences between signals.

One more important feature of the PLM is its insensitivity to volume conduction. This is very important when applying such metric to real data to avoid overestimating connectivity with spurious interactions.

Lastly, we should notice that the largest meaningful frequency difference between coupled signals remains to be determined.

## V. Conclusions

In conclusion, in this paper we propose a new metric for the connectivity estimation of brain signals that we named Phase Linearity Measurement (PLM). Such metric is an evolution of the Phase Lag Index (PLI) in the sense that the PLM allows to capture connectivity between oscillators with slightly different frequencies, and it is more robust with respect to noise. In brief, we removed the hypothesis that the two connecting brain areas would be characterized by exactly

the same oscillatory property, thus designing the PLM in order to consider also linear trends in the phase difference between signals. Such trends in the frequency domain are indeed used in order to estimate connectivity between signals. The results are encouraging and, compared to both the PLI and the AEC, the connectivity matrix estimations are very reliable. These findings suggest that the PLM might be well suited for reaching subject - level connectivity estimation.

## ACKNOWLEDGMENT

Authors would like to thank Prof. C. J. Stam for the valuable comments and suggestions.

## REFERENCES

[1] C. J. Stam, "Modern network science of neurological disorders," *Nature Rev. Neurosci.*, vol. 15, no. 10, pp. 683–695, 2014.
[2] E. Bullmore and O. Sporns, "Complex brain networks: Graph theoretical analysis of structural and functional systems," *Nature Rev. Neurosci.*, vol. 10, no. 3, pp. 186–198, Mar. 2009.
[3] K. J. Friston, "Functional and effective connectivity in neuroimaging: A synthesis," *Human Brain Mapping*, vol. 2, nos. 1–2, pp. 56–78, 1994.
[4] R. E. Greenblatt, M. E. Pflieger, and A. E. Ossadtchi, "Connectivity measures applied to human brain electrophysiological data," *J. Neurosci. Methods*, vol. 207, no. 1, pp. 1–16, May 2012.
[5] A. K. Engel, C. Gerloff, C. C. Hilgetag, and G. Nolte, "Intrinsic coupling modes: Multiscale interactions in ongoing brain activity," *Neuron*, vol. 80, no. 4, pp. 867–886, 2013.
[6] A. M. Bastos and J.-M. Schoffelen, "A tutorial review of functional connectivity analysis methods and their interpretational pitfalls," *Frontiers Syst. Neurosci.*, vol. 9, p. 175, Jan. 2016.
[7] G. Buzsaki, *Rhythms of the Brain*. London, U.K.: Oxford Univ. Press, 2006.
[8] P. Tass *et al.*, "Detection of $n : m$ phase locking from noisy data: Application to magnetoencephalography," *Phys. Rev. Lett.*, vol. 81, p. 3291, Oct. 1998.
[9] Y. Kuramoto, "Collective synchronization of pulse-coupled oscillators and excitable units," *Phys. D, Nonlinear Phenomena*, vol. 50, no. 1, pp. 15–30, 1991.
[10] S. H. Strogatz, "From Kuramoto to Crawford: Exploring the onset of synchronization in populations of coupled oscillators," *Phys. D, Nonlinear Phenomena*, vol. 143, nos. 1–4, pp. 1–20, 2000.
[11] A. T. Winfree, "Biological rhythms and the behavior of populations of coupled oscillators," *J. Theor. Biol.*, vol. 16, no. 1, pp. 15–42, 1967.
[12] R. M. Smeal, G. B. Ermentrout, and J. A. White, "Phase-response curves and synchronized neural networks," *Phil. Trans. Roy. Soc. London. B, Biol. Sci.*, vol. 365, no. 1551, pp. 2407–2422, 2010.
[13] F. L. da Silva, "EEG and MEG: Relevance to neuroscience," *Neuron*, vol. 80, no. 5, pp. 1112–1128, 2013.
[14] S. P. van den Broek, F. Reinders, M. Donderwinkel, and M. J. Peters, "Volume conduction effects in EEG and MEG," *Electroencephalogr. Clin. Neurophysiol.*, vol. 106, no. 6, pp. 522–534, 1998.
[15] P. S. Silva *et al.*, "Effect of field spread on resting-state magneto encephalography functional network analysis: A computational modeling study," *Brain Connectivity*, vol. 7, no. 9, pp. 541–557, 2017.
[16] G. Nolte, O. Bai, L. Wheaton, Z. Mari, S. Vorbach, and M. Hallett, "Identifying true brain interaction from EEG data using the imaginary part of coherency," *Clin Neurophysiol.*, vol. 115, no. 10, pp. 2292–2307, 2004.
[17] C. J. Stam, G. Nolte, and A. Daffertshofer, "Phase lag index: Assessment of functional connectivity from multi channel EEG and MEG with diminished bias from common sources," *Human Brain Mapping*, vol. 28, no. 11, pp. 1178–1193, 2007.
[18] G. L. Colclough, M. W. Woolrich, P. K. Tewarie, M. J. Brookes, A. J. Quinn, and S. M. Smith, "How reliable are MEG resting-state connectivity metrics?" *NeuroImage*, vol. 138, pp. 284–293, Sep. 2016.
[19] W. Singer, "Neuronal synchrony: A versatile code for the definition of relations?" *Neuron*, vol. 24, no. 1, pp. 49–65, 1999.
[20] M. Vinck, R. Oostenveld, M. van Wingerden, F. Battaglia, and C. M. A. Pennartz, "An improved index of phase-synchronization for electrophysiological data in the presence of volume-conduction, noise and sample-size bias," *NeuroImage*, vol. 55, no. 4, pp. 1548–1565, 2011.
[21] A. Bruns, R. Eckhorn, H. Jokeit, and A. Ebner, "Amplitude envelope correlation detects coupling among incoherent brain signals," *Neuroreport*, vol. 11, pp. 1509–1514, May 2000.
[22] B. C. M. van Wijk, C. J. Stam, and A. Daffertshofer, "Comparing brain networks of different size and connectivity density using graph theory," *PLoS ONE*, vol. 5, no. 10, p. e13701, 10 2010.
[23] G. Nolte, T. Holroyd, F. Carver, R. Coppola, and M. Hallett, "Localizing brain interactions from rhythmic EEG/MEG data," in *Proc. 26th Annu. Int. Conf. IEEE Eng. Med. Biol. Soc. (IEMBS)*, vol. 1, Sep. 2004, pp. 998–1001.
[24] M. Rosenblum, A. Pikovsky, J. Kurths, C. Schäfer, and P. A. Tass, "Phase synchronization: From theory to data analysis," *Handbook Biol. Phys.*, vol. 4, pp. 279–321, Aug. 2001.
[25] M. Yu, A. Hillebrand, A. A. Gouw, and C. J. Stam, "Horizontal visibility graph transfer entropy (HVG-TE): A novel metric to characterize directed connectivity in large-scale brain networks," *NeuroImage*, vol. 156, pp. 249–264, Aug. 2017.
[26] S. Rombetto, C. Granata, A. Vettoliere, and M. Russo, "Multichannel system based on a high sensitivity superconductive sensor for magnetoencephalography," *Sensors*, vol. 14, no. 7, pp. 12114–12126, 2014.
[27] P. K. Sadasivan and D. N. Dutt, "SVD based technique for noise reduction in electroencephalographic signals," *Signal Process.*, vol. 55, no. 2, pp. 179–189, 1996.
[28] G. Barbati, C. Porcaro, F. Zappasodi, P. M. Rossini, and F. Tecchio, "Optimization of an independent component analysis approach for artifact identification and removal in magnetoencephalographic signals," *Clin. Neurophysiol.*, vol. 115, no. 5, pp. 1220–1232, 2004.
[29] M. Fraschini, M. Demuru, A. Crobe, F. Marrosu, C. J. Stam, and A. Hillebrand, "The effect of epoch length on estimated EEG functional connectivity and brain network organisation," *J. Neural Eng.*, vol. 13, no. 3, p. 036015, 6 2016.
[30] R. Oostenveld, P. Fries, E. Maris, and J.-M. Schoffelen, "FieldTrip: Open source software for advanced analysis of MEG, EEG, and invasive electrophysiological data," *Comput. Intell. Neurosci.*, vol. 2011, Jan. 2011, Art. no. 1.
[31] B. D. van Veen, W. van Drongelen, M. Yuchtman, and A. Suzuki, "Localization of brain electrical activity via linearly constrained minimum variance spatial filtering," *IEEE Trans. Biomed. Eng.*, vol. 44, no. 9, pp. 867–880, Sep. 1997.
[32] N. Tzourio-Mazoyer *et al.*, "Automated anatomical labeling of activations in SPM using a macroscopic anatomical parcellation of the MNI MRI single-subject brain," *NeuroImage*, vol. 15, no. 1, pp. 273–289, 2002.